

Management of Cerebral Aneurysm Descriptors based on an Automatic Ostium Extraction

Monique Meuschke
University of Magdeburg

Tobias Günther
ETH Zürich

Ralph Wickenhöfer
Heart of Jesus Hospital,
Dernbach

Markus Gross
ETH Zürich

Bernhard Preim
University of Magdeburg

Kai Lawonn
University of Koblenz-
Landau

We present a framework to manage cerebral aneurysms. Rupture risk evaluation is based on manually extracted descriptors, which is time-consuming. Thus, we provide an automatic solution by considering several questions: How can expert knowledge be integrated? How should metadata be defined? Which interaction techniques are needed for data exploration?

Cerebral aneurysms are abnormal dilatations of intracranial arteries. Their rupture leads to subarachnoid hemorrhage (SAH) and is associated with a high mortality and morbidity rate. Most aneurysms are unintentionally detected due to

increased diagnostics. Even though most aneurysms will never rupture, they are usually treated, due to the poor prognosis of SAH. The associated risk of severe complications is considerable and can exceed the natural rupture risk.¹

For decision-making, the individual rupture risk is evaluated, which depends on different factors that are not yet well understood. To estimate risk factors, morphological descriptors such as aneurysm size are compared between ruptured and unruptured cases. The problem of analyzing aneurysm data is twofold. First, descriptors are manually extracted from clinical images, which is an error-prone process. An example for such descriptors is the width of the ostium, which separates the aneurysm from the parent vessel. Secondly, performing large medical studies with different domain experts is challenging, since different tools with inconsistent data formats are used. Thus, time is wasted to manually augment acquired data with meta information.

We present a framework that overcomes these problems. We introduce a novel approach to extract the ostium automatically and provide interaction techniques that allow an efficient manu-

al adaption of the automatic results. Based on this, we compute several morphological descriptors automatically and visualize them within the aneurysm. Our tool documents the aneurysm data in a consistent format. With this, users can search for specific cohorts, where individual cases can be analyzed in more detail to find possible rupture-prone correlations between morphological descriptors. In summary, our main contributions are:

- an automatic extraction of morphological descriptors, including the ostium; and
- a concept to consistently document and explore aneurysm data.

RELATED WORK

Related methods focus on structured documentation of clinical data and methods for the computer-assisted extraction of morphological descriptors of aneurysms.

Computer-Based Documentation

In clinical practice, reports describe patient state, diagnosis, and treatment recommendations, and serve for communication between referring clinicians. Due to their free-text form, they generally lack structure and readability. To improve this, *structured reports* were developed. Karim et al. provided clinical information using a Web-based application to generate structured reports for aortic aneurysms.² Visual analytics techniques support a more advanced collaborative analysis of medical datasets. To manage large volume segmentations in neuroscience, Ai-Awami et al. presented a Web-based system in which users have different permissions to edit and verify results.³ Bannach et al. combined medical image analysis with visual analytics to build, filter, analyze, and evaluate patient cohorts.⁴ Existing systems concentrate on the analysis and structured management of clinical image data. However, to investigate cerebral aneurysms, simulation data or geometry data has to be included. Therefore, we introduce a consistent format that allows analyzation of clinical, simulated, and reconstructed aneurysm data.

Extraction of Morphological Features

Medical research involves a detailed quantitative and qualitative analysis of specific anatomy and flow characteristics. To support such an analysis, it is necessary to derive morphological descriptors from the aneurysm data. A common descriptor is the vessel centerline, which can be obtained by thinning methods, distance transformations or Voronoi diagrams. From the aneurysm ostium, other important morphological descriptors are derived. Its maximum width, called neck width, was linked to rupture risk and treatment success. Karmonik et al. introduced an image-based method.⁵ They calculated centerline points for each image slice, fitted circles to cross-sections of the parent artery and determined the ostium by a radius analysis. Wong et al. used cylindrical surface models to reconstruct the normal vasculature.⁶ Another approach is to employ a Voronoi diagram of the surface to calculate a geodesic curve describing the ostium.^{7,8} Other researchers used deformable contour models to extract the ostium.⁹⁻¹¹ Neugebauer et al. employed the centerline and a manually defined point on the aneurysm to determine four points on the ostium using a geodesic distance metric.¹² Jerman et al. introduced a ray-casting approach, where rays are emitted from the aneurysm center towards the vessel wall.¹³ Based on the intersection distance, ostium points are detected. These methods fail for aneurysms with small arteries around the ostium or for wide neck aneurysms, as the cross-section of the ostium exceeds the aneurysm width.

In addition, some research groups use in-house tools to compute the aneurysm size or diameter automatically.^{14,15} However, these tools need manually extracted input data, e.g., centerlines. In contrast, we calculate morphological descriptors based on an automatically calculated ostium, where no further input data is needed. Moreover, our approach overcomes limitations for wide neck aneurysms and small arteries around the ostium.

DATA ACQUISITION

Our ostium extraction is based on a 3D polygonal mesh of the aneurysm surface reconstructed from 3D digital subtraction angiography. The vessel surface reconstruction is performed using the pipeline by Mönch et al.¹⁶ First, the aneurysm is segmented. Due to contrast agents, the clinical images exhibit a high vessel-to-tissue contrast. Thus, a threshold-based segmentation followed by a connected component analysis can be applied to separate the aneurysm and its parent vessel from the surrounding tissue. From the binary segmentation, the 3D vessel surface is extracted via Marching Cubes. To ensure anatomical accuracy, the 3D reconstructions were manually corrected by comparing with contours in the corresponding 2D slices.

REQUIREMENT ANALYSIS

The time-preserving management and exploration of aneurysm data, as well as a robust calculation of morphological descriptors has to fulfill several requirements that were gathered based on close cooperation with a neuroradiologist (16 years work experience), who regularly treats cerebral aneurysms, and an engineer working on simulations for cerebral aneurysms (four years work experience).

Currently, different pre- and post-operative data is acquired and stored on an FTP server in Microsoft Excel tables. Domain experts analyze the data collaboratively, which is time-consuming, since no consistent storage structure exists. Searching for specific cohorts, e.g., male patients with a ruptured aneurysm larger than 5 mm, is cumbersome. Thus, medical studies to investigate risk factors are difficult to carry out. Morphological descriptors are determined manually from 2D image slices using clinical software, or from 3D surfaces using the open-source program ParaView. ParaView is also used to manually extract the aneurysm ostium, which requires a tedious placement of cutting planes. We summarize the requirements as follows:

- **Requirement 1.** Methods are needed to integrate new datasets fast, including different meta information and data files.
- **Requirement 2.** We need a consistent structure for data management that can incorporate new data types if necessary.
- **Requirement 3.** An easy and fast editing of datasets is required, including quantitative parameters and data files.
- **Requirement 4.** Filter techniques are needed, which allow the selection of cohorts according to defined criteria.
- **Requirement 5.** An automatic calculation of morphological descriptors is needed, including the ostium.
- **Requirement 6.** Visualize the reconstructed and calculated components, e.g., 3D vessel surface or aneurysm ostium.

DETERMINATION OF MORPHOLOGICAL DESCRIPTORS

This section describes the automatic extraction and visualization of morphological descriptors, including the ostium. An automatic calculation of these features based on 2D clinical image data would require an automatic detection of aneurysms. However, recent approaches have still problems with false detections as well as missed detections and a reliable 2D ostium extraction is also challenging.^{17,18}

Extraction of the Aneurysm Ostium

To identify correlations between morphological descriptors and rupture, many datasets have to be analyzed, which requires a fast descriptor extraction. An important descriptor is the aneurysm ostium. Due to the lack of a unified definition, the ostium extraction is challenging. The ostium can be seen as an imaginary surface that separates the aneurysm sac from the non-pathologic parent vessel. Thus, the vessel structure without an aneurysm needs to be predicted. Most detec-

tion algorithms need a priori knowledge, e.g., the centerline of the parent vessel or user interaction, such as selecting the dome point, see Figure 1. To avoid such dependencies on pre-calculated data, we developed an efficient automatic extraction algorithm that provides facilities for an interactive correction of the result.

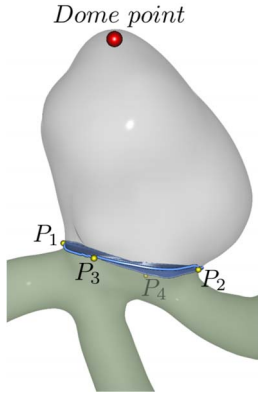


Figure 1. Four landmarks (P_1 to P_4) are connected by a curve to extract the ostium surface.

For extraction, a more geometric definition of the ostium is needed. We used the description of Neugebauer et al., who defined the ostium as a contour comprising four landmarks, P_1 to P_4 (see Figure 1).¹² The first two points, P_1 and P_2 , are located on the transition between the aneurysm and parent vessel. The other two landmarks control the bending of the ostium around the parent vessel. The goal is to identify these four points. Our algorithm consists of six steps, as described in the following.

Skeleton Extraction. Before we are able to compute the precise positions of P_1 to P_4 , we have to estimate which vessel part represents the aneurysm. Therefore, we used the skeleton of the aneurysm and parent vessel geometry determined using the method by Au et al.¹⁹ This method performs automatically and thus, no a priori knowledge is needed as input data. Iterative implicit Laplacian smoothing is applied to generate a zero-volume skeletal shape. Global positional constraints are defined to preserve the connectivity, which yields curves that represent the vessel skeleton. Afterwards, each skeleton vertex corresponds to faces (and vertices) of the surface.

Aneurysm Identification. In the second step, we use the skeleton to identify the aneurysm vessel part. The nodes of the vessel skeleton can be characterized according to their number of outgoing edges: end nodes (one edge), mid nodes or non-junction nodes (two edges) and junction nodes (more than two edges). Junction nodes occur at bifurcations of the original surface. We determine all end nodes and for each, the nearest junction node is searched by traversing the skeleton. We have to decide if the path from the end node to the junction node (over mid nodes) represents a section of the parent vessel or the aneurysm. These paths inherit a corresponding amount of vertices on the original surface. For these vertices, we compute the shape index

$$S_i = \frac{1}{2} - \frac{1}{\pi} \arctan \left(\frac{K_1 + K_2}{K_1 - K_2} \right)$$

and average them, with $K_1 \geq K_2$ being the principal curvatures. Since aneurysms are usually spherical structures, skeleton sections representing the aneurysm exhibit a higher S_i than sections representing the elongated parent vessel. Based on this assumption, we determine the junction P_{AJ} (green) and end node P_{AE} (red), representing the aneurysm, see Figure 2a bottom. Thus, inaccuracies due to small arteries around the ostium are avoided. In case the highest S_i does not represent the aneurysm (did not occur in our cases), the user can correct the detection by selecting the correct end node P_{AE} .

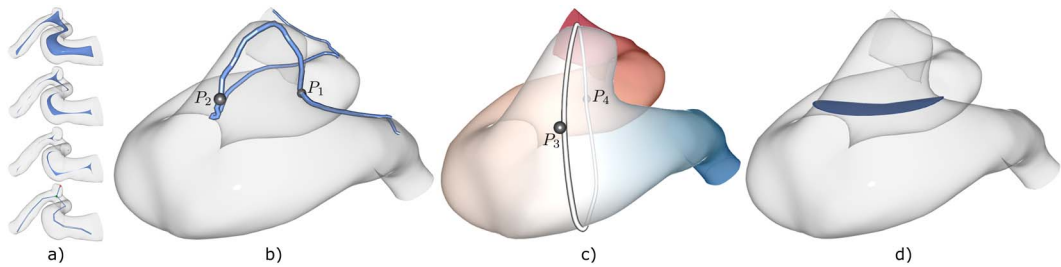


Figure 2. Pipeline for the ostium reconstruction. First, the vessel skeleton is calculated by iteratively shrinking the surface mesh. The skeleton is projected on the aneurysm and two points P_1 and P_2 are determined (b), which are used to compute a distance field d_3 , color-coded on the surface. Based on the isoline $d_3 = 0$, two more points P_3 and P_4 are determined (c). Finally, P_1 to P_4 are connected to a curve to extract the ostium surface.

Extraction of P_1 and P_2 . Based on the detected aneurysm vessel part, we identify the first two landmarks P_1 and P_2 by generating a curve on the vessel over the aneurysm, see Figure 2(b). Inspired by Neugebauer et al., who project the centerline on the surface along the vector pointing from the centerline to the aneurysm's dome,¹² we determine another curve on the surface that provides us with P_1, P_2 . This information is employed by first determining the path from the junction node to the remaining end nodes (except the end node, corresponding to the aneurysm). If more than two paths exist, we determine the first tangent vector of each path by subtracting the coordinate of the first neighbor node of the junction node and the junction node itself. For each of these vectors, we calculate the enclosing angle with $P_{AE}-P_{AJ}$. The two paths, which are closest to 90° are used for further consideration. Then, the Euclidean distances between the surface points, belonging to the current node of the skeleton path and the point P_{AE} are determined. This is performed for all skeleton nodes, where the vertices representing the minimal distance are connected using the Dijkstra algorithm w.r.t. neighbored nodes of the skeleton. This yields a path f on the aneurysm surface, see Figure 2b. Afterward, the global minima, which represents the aneurysm's dome position is determined. For f_1 and f_2 , we determine the positions where the distance to the junction node is minimal, which yields the landmarks P_1 and P_2 , see Figure 2b. For aneurysms with more than two outgoing vessels, more ostium points are detected, where we take the two with the maximum occurring distance for P_1 and P_2 .

Extraction of P_3 and P_4 . To define a contour that represents the correct bending of the aneurysm, two more landmarks P_3 and P_4 are needed, where all landmarks should be evenly distributed throughout the ostium contour. For this, P_1 and P_2 are connected using the Dijkstra algorithm. On this path, P_3 is determined so that P_3 has the same distance to P_1 and P_2 . These three points define a plane E . Then, we calculate two geodesic distance fields d_1 and d_2 .²⁰ The first distance field starts at P_1 and the second starts at P_2 . Based on d_1 and d_2 , we compute a third distance field $d_3 = d_1 - d_2$. To get P_4 , we determine the isoline I representing $d_3 = 0$ that lies between P_1 and P_2 , and compute the intersection points between I and E . From these points, we take the intersection point S_3 that has the larger distance to P_3 to fulfill the condition of evenly distributed landmarks. From S_3 , we go along I in the direction of the smaller distance from P_{AJ} . This minimum represents P_4 , see Figure 2c.

Ostium Extraction. P_1 to P_4 are connected to a curve C_{ostium} using the method by Surazhsky,²¹ determining the shortest geodesic path between points on a triangular mesh. Finally, the enclosing area, representing the ostium surface is triangulated by determining the mean point P_{mean} , where adjacent points on C_{ostium} form a triangle with P_{mean} , see Figure 2d.

Ostium Correction. Due to the anatomical diversity, P_1 to P_4 are not always optimal. Therefore, the user can select other positions on the mesh to correct C_{ostium} . Figure 3a shows the automatically calculated ostium surface, where P_1 to P_4 are rendered as yellow spheres. For selecting a new point P_{new} , we determine which of P_1 to P_4 has the smallest geodesic distance to P_{new} . Then, P_{new} replaces this ostium point, the corresponding contour parts are recalculated and a new triangulation of the ostium surface is generated, while the old ostium point is depicted semi-transparently, see Figure 3b. The recalculation takes less than 1 s.

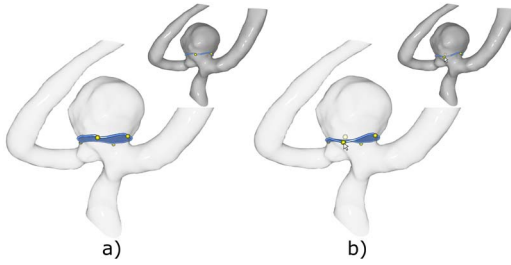


Figure 3. Manual ostium correction. By selecting new points on the mesh, the ostium is adjusted, where the blue point is depicted semi-transparently.

Calculation of Quantitative Parameters

Based on the extracted ostium and the dome point, we compute seven 1D and five 2D morphological descriptors to investigate the rupture risk! The 1D descriptors are aneurysm height (H), maximum width (W_{max}), maximum diameter (D_{max}), neck width (W_{neck}), and bulge height (H_{bulge}), the height from ostium to the plane of (W_{max}), parent artery diameter (D_{parent}), and the angle between parent artery and aneurysm apex (A_{pa}). The 2D descriptors are aspect ratio (H/W_{neck}), height-width ratio (H/W_{max}), bottleneck factor (W_{max}/W_{neck}), bulge location (H_{bulge}/H) and aneurysm/parent artery ratio (D_{max}/D_{parent}). The length of vector $\mathbf{v}_h = \mathbf{p}_d - \mathbf{p}_o$ with dome point \mathbf{p}_d and ostium center \mathbf{p}_o represents $H = \|\mathbf{v}_h\|$. To calculate W_{max} for each vertex of the aneurysm \mathbf{v}_i , we determine the corresponding point \mathbf{p}_i on \mathbf{v}_h : $\mathbf{p} = \mathbf{p}_o + \frac{(\mathbf{v}_i - \mathbf{p}_o) \cdot (\mathbf{v}_h)}{\|\mathbf{v}_h\|^2} \mathbf{v}_h$. Using \mathbf{p}_i , a ray r is defined: $r = \mathbf{p}_i + t(\mathbf{p}_i - \mathbf{v}_i)$. Based on r , all intersection points with the aneurysm surface are calculated and the intersection \mathbf{v}_j with the greatest Euclidean distance to \mathbf{p}_i is used to calculate $W_{max} = \|\mathbf{v}_j - \mathbf{p}_i\|$. The maximum diameter is given by the two aneurysm points \mathbf{v}_i and \mathbf{v}_j with the greatest Euclidean distance. Similarly, W_{neck} is defined as the maximum Euclidean distance between two points belonging to the aneurysm ostium. To calculate the bulge height, we use: $H_{bulge} = \|\mathbf{p}_i - \mathbf{p}_o\|$. From the skeletonization the vessel diameter is known at each node. We assign the median radius to D_{parent} . To compute A_{pa} , \mathbf{v}_h and the nearest skeleton node to the ostium center \mathbf{c}_p , as well as the tangent \mathbf{t} at this point are used. The angle between \mathbf{v}_h and \mathbf{t} is A_{pa} .

Visualization of Morphological Criteria

On the semi-transparent vessel surface, morphological descriptors are shown. For 1D descriptors, the defining endpoints are rendered as spheres. Their connecting line is shaded as tube to improve its perception,²² see Figure 4. For 2D descriptors, the corresponding 1D structures are depicted. Users can activate individual descriptors.

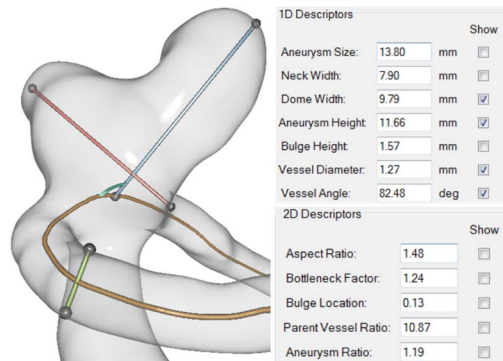


Figure 4. Visualization and quantitative values of morphological descriptors, showing W_{max} (red), H (blue), D_{parent} (light green) and A_{pa} (dark green semi-circle).

MANAGEMENT OF ANEURYSM DATA

To better understand the patient-specific rupture risk and to find an optimal treatment, a large number of ruptured and non-ruptured datasets have to be compared. For this, different types of data such as image or flow data as well as morphological descriptors or patient-specific meta information have to be analyzed. Therefore, we developed a consistent structure for handling aneurysm data that avoids redundancy. Besides the visualizations, other exploration techniques are provided to manage and analyze the data.

Documentation Structure

Our framework consists of three parts: a database, an FTP server and a visualization component. The acquired image data is stored on the FTP server, using the data structure shown in Figure 5. For each patient, a new case is created on the server, with pre- and post-operative data that is organized in studies. Each study comprises four information elements: Scanner data includes CTA and MRA data. Geometric information is stored in reconstruction data, e.g., the ostium. Moreover, flow simulations are stored, for either single (steady) or multiple (unsteady) time steps. Different formats such as Ensignt or OpenFoam are distinguished. Media data contains characteristic images or videos, e.g., showing wall regions with higher risk. In addition, meta data is stored for the cases, studies and corresponding data items, including the study type (patient or proband), gender and age. Furthermore, the morphological descriptors, information about rupture and treatment are collected.

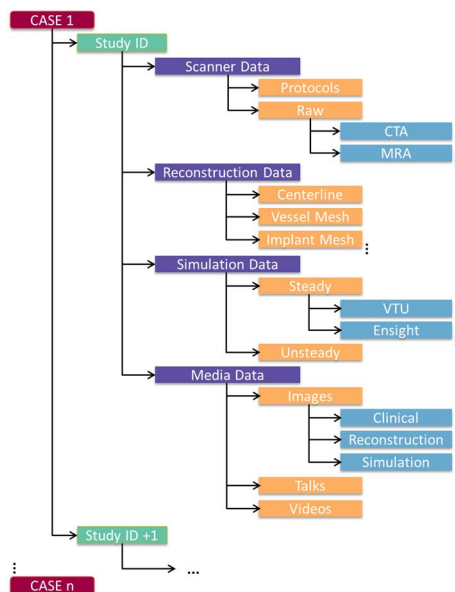


Figure 5. Data structure on the FTP server. Each case conforms to a patient or proband. Data items acquired at different times are coordinated into studies.

The visualization component provides an overview depiction of existing cases using a tabular representation. Besides basic case information, a preview picture of an optimal view on the aneurysm surface is shown, generated with the method by Meuschke et al.,²³ see Figure 6. Moreover, widgets to add and edit cases and studies, download data from the FTP server or to render the 3D reconstructed data are provided.

Interaction Techniques

To search for specific cohorts, configurable filtering masks are provided. Figure 6 shows two masks, where users can select study information (left, top) and aneurysm descriptors (left, bot-

tom). Datasets that do not satisfy the selected criteria are removed from the tabular overview. Pressing the edit button (see Figure 6, bottom right) displays a summary of meta information including available data on the FTP server, see Figure 7, and enables editing such as adding of aneurysm descriptors. Besides directly editing morphological descriptors, users can activate the 3D visualization. When manually correcting the ostium, the morphological descriptors are recalculated and stored.

View	Case	Study	Study Tag	City	Pathology	Date	Scanner Data	Reconstruction Data	Simulation Data	Media Data
	2	1	Expanded Neck	Magdeburg	Aneurysm	11.04.2017	existent	existent	existent	existent
	3	1	Bifurcation Aneurysm	Magdeburg	Aneurysm	11.04.2017	existent	existent	not existent	not existent
	4	1	Multiple Blebs	Magdeburg	Aneurysm	15.04.2017	existent	existent	not existent	not existent
	5	1	Multiple Aneurysm	Magdeburg	Aneurysm	23.04.2017	existent	existent	existent	not existent
	5	2	Multiple Aneurysm	Magdeburg	Aneurysm	23.04.2017	existent	existent	not existent	not existent
	6	1	Multiple Aneurysm	Magdeburg	Aneurysm	01.06.2017	existent	existent	not existent	existent
	6	2	Multiple Aneurysm	Magdeburg	Aneurysm	01.06.2017	existent	existent	existent	not existent
	7	1	Bifurcation Aneurysm	Magdeburg	Aneurysm	12.06.2017	existent	existent	not existent	not existent
	8	1	Clemens_Data	Magdeburg	Aneurysm	25.06.2017	existent	existent	existent	existent

Figure 6. Datasets are shown in a tabular representation. On the left, filtering masks are provided to search for cohorts.

Case Data
Case No.: 2 Study No.: 1
Tags: Bifurcation Aneurysm
City: Magdeburg Uploader:
Date: 11.04.2017 Type: Patient
Gender: Female Age: 55
Acquisition: Magdeburg

Pathology Data
Pathology: Aneurysm
Properties: Form: Saccular Position: Middle Cerebral Artery Height: 4.5 mm
Files:
Tags: Aneurysm with wide neck

Scanner Data

ID	Data Type	Modality	Image Type	Treatment Time	Tags
Raw	CTA	Composed	Pra-Treat.		
Raw	MRA	Composed	Pra-Treat.		

Reconstruction Data

Data Category	Tags
Vessel Mesh	
Implant Mesh	

Simulation Data

Data Type	Option	Tags
Steady	VTU	

Media Data

Data Category	Data Type	Tags

Download Visualize Upload

Figure 7. User interface to manage and explore aneurysm data. Existing data is summarized and can be edited.

EVALUATION

To show the improved accuracy of automatically calculated results, we compare the calculated morphological descriptors with manually measured descriptors provided by two neuroradiologists. Moreover, we compare our ostium extraction with manual expert results and with the results of an existing approach. Finally, informal interviews with four domain experts are performed to evaluate the implementation of the defined requirements.

Comparison to Expert Results

The experts manually determined the morphological 1D descriptors based on CTA slice images for 10 datasets. Moreover, the manual measurements were performed on the 3D surface mesh. Therefore, they selected points on the surface that define the endpoints of the descriptors. The angle A_{pa} could not be measured in 2D, because it is challenging to find an appropriate slice. We compared the manual 2D (2DM) and 3D (3DM) measurements to our 3D automatic computations (3DA), see Table 1. In medical guidelines, an increased rupture risk is assumed for aneurysms larger than 7 mm and therefore, they are usually treated. Moreover, the experts stated that measurement deviations of more than 0.5 mm would be critical, since this could influence the treatment decision.

Table 1. Comparison of our automatically calculated (3DA) descriptors to manually measurements based on 2D image slices (2DM) and the 3D aneurysm surface (3DM). Maximum occurred deviations are emphasized.

Criteria	Measure	D1	D2	D3	D4	D5	D6	D7	D8	D9	D10
Height (mm)	2DM	7.8	3.8	6.0	4.5	5.0	4.6	4.1	4.6	5.3	4.7
	3DM	8.4	3.7	5.3	4.4	5.7	5.9	4.5	4.1	5.1	4.6
	3DA	8.5	4.1	5.5	4.8	5.7	6.1	4.6	4.4	5.4	4.9
Width (mm)	2DM	4.2	3.4	5.3	4.5	5.4	4.5	3.8	4.8	3.0	4.2
	3DM	5.7	3.2	4.8	5.3	6.7	6.5	4.7	4.7	4.3	5.1
	3DA	5.8	3.6	4.9	5.5	7.0	6.7	4.8	5.0	5.1	5.2
Diameter (mm)	2DM	9.1	4.4	6.2	4.5	5.5	5.5	4.4	5.0	6.1	5.7
	3DM	9.9	4.9	6.3	6.5	7.6	6.7	5.0	4.8	6.3	6.5
	3DA	10.7	5.3	6.4	6.8	7.7	7.4	5.6	5.2	7.0	6.9
Neck Width (mm)	2DM	3.6	2.1	1.4	4.6	3.4	2.7	2.3	2.4	2.5	3.3
	3DM	3.6	2.3	2.0	4.5	3.6	3.5	3.0	2.8	3.2	4.1
	3DA	4.4	2.7	2.5	4.9	4.4	4.1	3.0	2.8	3.4	4.3
Bulge Height (mm)	2DM	7.0	1.5	3.0	2.2	2.9	3.0	1.4	0.9	0.8	1.0
	3DM	6.7	1.4	2.8	2.6	4.0	2.9	1.6	1.3	0.8	0.9
	3DA	6.4	1.4	2.9	1.3	3.1	3.3	1.7	2.2	1.0	1.1
Artery Diameter (mm)	2DM	1.0	1.0	0.6	0.8	0.7	0.9	1.1	0.9	1.2	0.9
	3DM	1.0	1.0	0.6	0.9	0.7	0.8	1.0	0.7	1.2	1.1
	3DA	1.2	1.0	0.7	0.9	0.8	0.8	1.0	0.8	1.3	1.1
Apex Angle (degrees)	2DM	x	x	x	x	x	x	x	x	x	x
	3DM	50.6	60.7	55.2	49.9	51.4	80.6	60.3	75.5	48.3	77.3
	3DA	45.8	54.7	41.8	38.1	59.8	89.5	44.6	80.1	54.4	83.4

Measurement deviations differ for the individual descriptors. For height, the maximum difference between 2DM and 3DM is 1.3 mm and between 2DM and 3DA is 1.5 mm. However, between 3DM and 3DA, the deviation was reduced to 0.4 mm. Similar differences occurred for the

bulge height that has a maximum difference of 1.1 mm, 1.3 mm and 1.3 mm for 2DM/3DM, 3DM/3DA and 2DM/3DA. The aneurysm width and diameter show larger deviations between 2DM/3DA with 2.2 mm and 2.3 mm, which are highly critical deviations according to treatment decision. Also the median differences are increased with 1 mm for width and 1.2 mm for diameter. For 3DM/3DA, a maximum difference of 0.8 mm occurs for both. The neck width shows a maximum difference of 0.8 mm between 2DM/3DM and 3DM/3DA, but between 2DM/3DA a maximum deviation of 1.4 mm occurred. The measurements for A_{pa} exhibit a maximum difference of 15.7 degrees between 3DM/3DA. For the parent artery diameter, the lowest maximum differences occurred with 0.1 mm, 0.2 mm and 0.1 mm for 2DM/3DM, 3DM/3DA and 2DM/3DA.

Evaluation of the Ostium Extraction

To assess the quality of our ostium extraction, we compare the calculated ostium contours using the Hausdorff distance H_d to ostium curves, manually defined on the 3D aneurysm mesh by medical experts, see Table 2 (first row). The experts selected points on the surface that were connected by the method of Surazhsky.²¹

Table 2. Hausdorff distance between the automatically and manually generated ostium as well as deviations for the morphological descriptors calculated based on both ostium surfaces.

Criteria	D1	D2	D3	D4	D5	D6	D7	D8	D9	D10
Hausdorff (mm)	0.35	0.61	0.31	0.19	0.31	0.38	0.25	0.40	0.75	0.39
Height (mm)	0.07	0.23	0.05	0.01	0.35	0.12	0.01	0.01	0.33	0.1
Width (mm)	0	0.23	0.09	0.02	0.03	0.01	0	0.01	0.61	0.1
Diameter (mm)	0	0.54	0.14	0.23	0	0.22	0	0	0.27	0.03
Neck Diameter (mm)	0.14	0.43	0.08	0.07	0.05	0.23	0.04	0.21	0.28	0.05
Bulge Height (mm)	0.07	0.28	0.24	0.16	0.17	0.06	0.01	0.05	0.63	0.01
Apex Angle (degrees)	0.58	1.01	0.49	0.88	0.46	0.19	0.11	0.58	1.87	0.73

Our automatic approach and the manual approach lead to similar results. The maximum occurring H_d is 0.75 mm (D9), whereas the best result has a H_d of 0.19 mm (D4), both depicted in Figure 8. The aneurysm of D9 is parallel to the vessel, which leads to a similar distance to the skeleton. Thus, the applied distance metric returns no optimal positions for P_1 and P_2 . However, the experts stated that the correction of the ostium contour by selecting new points is easy to use and allows for a fast adaption. Furthermore, we investigated the influence of occurring deviations between the manually and automatically extracted ostium on morphological descriptors. Table 2 shows deviations of the descriptors calculated for both ostium surfaces. For D9, the maximum difference is 0.63 mm for the bulge height and for D2, the diameter deviates by 0.54 mm. The experts recommend a manual correction for a deviation of more than 0.5 mm. As for the angle differences, they were unsure about an acceptable variance because there are no studies that show a significant influence of the angle on the rupture risk. However, for the distance-based criteria, the comparison shows that our ostium extraction leads to appropriate results for the majority of the tested datasets.

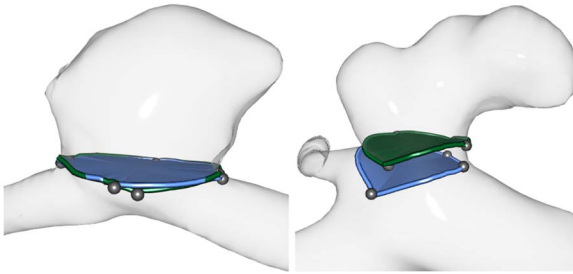


Figure 8. Automatic ostium results for D4 (left) and D9 (right) compared to the manual results (green), where the automatic and manual results are very close to each other in the left image.

We compared our method with the semi-automatic ostium extraction of Neugebauer et al.¹² Figure 9 shows two ostium surfaces with our approach (blue), with the semi-automatic method (red) and manually generated (green) for aneurysms with a wide neck. The semi-automatic method leads to very dissimilar results compared to manual surfaces due to a wrong determination of P_4 . Our method is much closer to the manually generated surfaces, which is reflected in the Hausdorff distances with 5.14 (left) and 1.67 mm (right) for the semi-automatic approach and 0.30 mm (left) and 0.48 mm (right) for our technique.

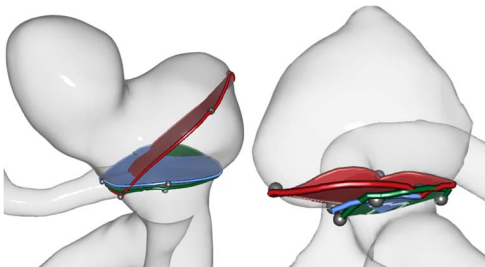


Figure 9. Comparison of our method (blue) to the semi-automatic approach [12] (red) and manual results (green).

Evaluation of the Data Administration

The workflow was designed and evaluated with two engineers with expertise in blood flow simulations, and the two neurologists. During the informal evaluation the following tasks were performed:

1. Adding a new case.
2. Adding a new study to an existing case, including information about the pathology.
3. Editing a study by uploading additional files and changing morphological descriptors.
4. Searching for a cohort that fulfills specific descriptors with a specified variance.

First, we described the functionality of the tool. Then, the experts performed the defined tasks, while we noted the experts' spoken comments.

Adding new cases and studies was described as simple by all experts (Requirement 1). The predefined drop down menus enable a fast selection of meta information. Short text-based descriptions can be added to cases and studies, for which experts wished for suggestions of already used descriptions. In addition, they emphasized the possibility to upload files for selected pathology information, i.e., images of aneurysm location or reports about rupture. Furthermore, the experts wished for an option to add new studies to the selected case in the main view.

For editing, the experts selected a case from the tabular overview. They were able to edit meta information and to upload different types of data using the predefined structure, see Figure 5 (Requirement 2). They liked the overview of already uploaded data which avoids redundancy. In

addition, they used the visualizations to explore and edit morphological descriptors. The automatic calculation was considered very helpful, as it saves time and avoids measurement errors (Requirement 5). They wished for a visual summary for clinical documentations and treatment planning.

Finally, the experts searched for specific cohorts. The predefined property lists enable a fast definition of individual filtering masks (Requirement 4). The possibility to define a permitted variance for each property was emphasized, as it allows a detailed analysis of ruptured and unruptured cases. The experts would like to have a statistical analysis of morphological descriptors within a filtered cohort.

DISCUSSION

Since we ensure anatomical accuracy during the vessel reconstruction, see “Data Acquisition” section, we interpret occurring deviations between manual and calculate descriptors as descriptor-dependent measurement errors. The aneurysm diameter and width show strong variations, since the maximum extent is difficult to find manually in 3D. Measuring aneurysm angles is almost impossible in 2D. In contrast, measurements of the parent artery diameter, which is independent of aneurysm shape, show the lowest deviations. Thus, manual measurements are error-prone and time-consuming. Processing a dataset took between 8–10 minutes, whereas our method needs 1.0–1.9 minutes. In clinical routine, such measurements are currently the basis for decision-making. Thus, aneurysms are treated that could initially be observed based on objective automatic measurements. This is important since treatment also carries considerable risk of severe complications. This aside, manual measurements are not reproducible. To better understand the rupture risk and to evaluate the aneurysm state over time as well as to find an optimal treatment, reproducible measurements are needed.

We compared our automatic ostium extraction with manually generated ostium contours and with the method by Neugebauer et al.¹² Our results are very similar to manual expert results and exhibit significantly lower Hausdorff distances than the results by Neugebauer et al.¹² Moreover, our approach is independent of predefined input data and overcomes limitations of existing approaches handling wide neck aneurysms and small arteries around the ostium.

However, our approach is limited to cases with one aneurysm. For multiple aneurysms (about 20% of all cases), ostium surfaces have to be computed separately. Moreover, problems occur if the aneurysm runs parallel to the parent artery, which is uncommon according to the medical experts. The medical literature provides no unique ostium definition leading to slightly different ostium curves by different domain experts. Thus, we calculated the variances of morphological descriptors between our automatic and the manually defined ostium. Except for two datasets, no significant changes occurred and thus our ostium calculations are appropriate to analyze the aneurysm morphology.

The informal study showed that our framework fulfills the defined requirements. All experts were able to efficiently use the tool and they would employ it for exploration and management of aneurysm data. To the best of our knowledge, there is no comparable concept that focuses on the management of aneurysm data, comprising clinical images, flow data, morphological descriptors and patient-specific meta information. Our tool allows for an efficient filtering of datasets, which supports the collaboration of different research groups. Furthermore, the descriptors are visualized in a qualitative and quantitative manner, which could also be used for documentation and patient education in clinical routine. The analysis of cohorts has to be further supported by statistical methods combined with visual analytics to provide a more detailed investigation of descriptors. This would also require techniques that allow for a visual comparison of multiple datasets.

CONCLUSION

We presented a tool for visual exploration and management of cerebral aneurysms. Based on an automatic ostium extraction, morphological descriptors are automatically calculated and investi-

gated, which is less time-consuming and error-prone than manual measurements. A consistent data structure was defined to ensure a redundancy-free storage of aneurysm data. Filtering of cohorts supports domain experts to better understand individual risk factors.

Until now, no percentage value could be calculated that reliably indicates rupture probability. Determining a value is challenging, since various factors influence the rupture, such as morphological descriptors and inflammation processes that cannot be modeled yet. Moreover, clinicians evaluate rupture risk differently based on their experience. Our tool enables a fast and objective analysis of the aneurysm morphology in clinical discussions by automatic calculations and data management.

In the future, we plan to use the morphological criteria to build an aneurysm rupture risk classification. Providing decision trees could support treatment decisions. Moreover, we intend to apply our ostium extraction to a larger amount of datasets to further evaluate its robustness. Therefore, further manual ostium extractions are required by domain experts. In addition, we want to compute the morphological descriptors for time-dependent data that consider the vessel deformation during the cardiac cycle. For this, visualization techniques would be needed that show the behavior of the parameters over time. Finally, we want to extend our ostium extraction to multiple aneurysms and integrate hemodynamic descriptors that also seem to influence the rupture risk.

ACKNOWLEDGMENTS

This work was partially funded by the BMBF (STIMULATE: 13GW0095A). The authors like to thank Philipp Berg, Samuel Voß, and Oliver Beuing for the fruitful discussions on these and related topics.

REFERENCES

1. B.L. Hoh et al., "Bottleneck factor and height-width ratio: association with ruptured aneurysms in patients with multiple cerebral aneurysms," *Neurosurgery*, vol. 61, no. 4, Oxford University Press, 2007, pp. 716–723.
2. S. Karim et al., "Development, implementation, and evaluation of a structured reporting web tool for abdominal aortic aneurysms," *JMIR Research Protocols*, vol. 2, no. 2, JMIR Publications Inc., 2013; doi.org/10.2196/resprot.2417.
3. A.K. Ai-Awami et al., "NeuroBlocks--Visual tracking of segmentation and proofreading for large connectomics projects," *IEEE Transactions on Visualization and Computer Graphics*, vol. 22, no. 1, IEEE, 2016, pp. 738–746.
4. A. Bannach et al., "Visual Analytics for Radiomics: Combining Medical Imaging with Patient Data for Clinical Research," *Workshop on Visual Analytics in Healthcare*, 2017.
5. C. Karmonik et al., "A technique for improved quantitative characterization of intracranial aneurysms," *American Journal of Neuroradiology*, vol. 25, no. 7, Am Soc Neuroradiology, 2004, pp. 1158–1161.
6. W.C.K. Wong and A.C.S. Chung, "Augmented vessels for quantitative analysis of vascular abnormalities and endovascular treatment planning," *IEEE Transactions on Medical Imaging*, vol. 25, no. 6, IEEE, 2006, pp. 665–684.
7. M.D. Ford et al., "An objective approach to digital removal of saccular aneurysms: technique and applications," *The British Journal of Radiology*, vol. 82, no. 1, The British Institute of Radiology, 36 Portland Place, London, W1B 1AT, 2009, pp. 55–61.
8. R. Cárdenes et al., "Automatic aneurysm neck detection using surface Voronoi diagrams," *IEEE Transactions on Medical Imaging*, vol. 30, no. 10, IEEE, 2011, pp. 1863–1876.
9. A. Mohamed et al., "Computer-aided planning for endovascular treatment of intracranial aneurysms," *Medical Imaging 2010: Visualization, Image-Guided Procedures, and Modeling*, International Society for Optics and Photonics, 2010; doi.org/10.1117/12.841042.

10. S. Hassan et al., "Automatic localization and quantification of intracranial aneurysms," *Computer Analysis of Images and Patterns*, Springer, 2011, pp. 554–562.
11. I. Larrabide et al., "Three-dimensional morphological analysis of intracranial aneurysms: A fully automated method for aneurysm sac isolation and quantification," *Medical physics*, vol. 38, no. 5, Wiley Online Library, 2011, pp. 2439–2449.
12. M. Neugebauer et al., "Geometric Reconstruction of the Ostium of Cerebral Aneurysms," *Vision, Modeling, Visualization*, 2010, pp. 307–314.
13. T. Jerman et al., "Computer-aided detection and quantification of intracranial aneurysms," *International Conference on Medical Image Computing and Computer-Assisted Intervention*, 2015, pp. 3–10.
14. S Dhar et al., "Morphology parameters for intracranial aneurysm rupture risk assessment," *Neurosurgery*, vol. 63, no. 2, Oxford University Press, 2008, pp. 185–197.
15. A. Lauric, M.I. Baharoglu, and A.M. Malek, "Ruptured status discrimination performance of aspect ratio, height/width, and bottleneck factor is highly dependent on aneurysm sizing methodology," *Neurosurgery*, vol. 71, no. 1, Oxford University Press, 2012, pp. 38–46.
16. T. Moench, M. Neugebauer, and B. Preim, "Optimization of vascular surface models for computational fluid dynamics and rapid prototyping," *Second International Workshop on Digital Engineering*, 2011.
17. A. Chandra and S. Mondal, "Amalgamation of iterative double automated thresholding and morphological filtering: a new proposition in the early detection of cerebral aneurysm," *Multimedia Tools and Applications*, Springer, 2016.
18. C.M. Hentschke et al., "A system to detect cerebral aneurysms in multimodality angiographic data sets," *Medical physics*, vol. 41, no. 9, Wiley Online Library, 2014.
19. O.K.-C. Au et al., "Skeleton extraction by mesh contraction," *ACM Transactions on Graphics*, vol. 27, no. 3, 2008, p. 44.
20. K. Crane, C. Weischedel, and M. Wardetzky, "Geodesics in Heat: A New Approach to Computing Distance Based on Heat Flow," *ACM Transactions on Graphics*, vol. 32, no. 5, 2013, p. 152.
21. V. Surazhsky et al., "Fast exact and approximate geodesics on meshes," *ACM Transactions on Graphics*, vol. 24, no. 3, 2005, pp. 553–560.
22. C. Stoll, S. Gumhold, and H.-P. Seidel, "Visualization with stylized line primitives," *IEEE Visualization 2005 (VIS 05)*, 2005.
23. M Meuschke et al., "Automatic Viewpoint Selection for Exploration of Time-Dependent Cerebral Aneurysm Data," *Bildverarbeitung fuer die Medizin 2017*, 2017, pp. 352–357.

ABOUT THE AUTHORS

Monique Meuschke is a Doctoral Research Fellow and affiliated with the research campus STIMULATE at the University of Magdeburg (UoM), Germany. In 2015, she received a master in Computational Visualistics from the UoM. Her research interests are the visual analysis, exploration and classification of medical blood flow data. Contact her at meuschke@isg.cs.uni-magdeburg.de.

Tobias Günther joined the Computer Graphics Laboratory (CGL) at the ETH Zurich as a postdoctoral researcher in 2016. He received his MSc in Computer Science in 2013 and his PhD in 2016, both from the UoM. His research interests include scientific visualization, progressive light transport and real-time rendering. Contact him at tobias.guenther@inf.ethz.ch.

Ralph Wickenhöfer is head of the clinic for Radiology and Nuclear Medicine at the Heart of Jesus Hospital in Dernbach, Germany. He is an MD since 1986 and scientific adviser for the Institute for Medical Technology and Information Processing at the University of Koblenz-Landau. His research interests are neural networks and machine learning. Contact him at r.wickenhoefer@krankenhaus-dernbach.de.

Markus Gross is a professor of computer science at the Swiss Federal Institute of Technology Zurich, head of the CGL, and the Director of Disney Research, Zurich. His research in-

terests include physically based modeling, computer animation, immersive displays, and video technology. He received a PhD in computer graphics and image analysis from Saarland University in 1989. Contact him at grossm@inf.ethz.ch.

Bernhard Preim has headed the Visualization Group at the University of Magdeburg (UoM) since 2003. Before that, he was a staff member at MEVIS Bremen. He received a PhD at the UoM in 1998 and a habilitation (*venia legendi*) in 2002 from the University of Bremen. His research interests are in medical visualization and applications in diagnosis and treatment. Contact him at bernhard@isg.cs.uni-magdeburg.de.

Kai Lawonn is an assistant professor for medical visualization at the University of Koblenz Landau. He studied Mathematics at the Freie University of Berlin and in 2014, he received his PhD in Computer Science from the UoM. His research interests are illustrative visualizations for medical and biological applications. Contact him at lawonn@uni-koblenz.de.